Acute and obtuse rhombohedrons in the local structures of relaxor ferroelectric Pb(Mg$_{1/3}$Nb$_{2/3}$)O$_3$

Wen Hu,[1,*] Kouichi Hayashi,[2,†] Kenji Ohwada,[1] Jun Chen,[3] Naohisa Happo,[4] Shinya Hosokawa,[5] Masamitu Takahasi,[1] Alexei A. Bokov,[6] and Zuo-Guang Ye[6,‡]

[1]*Quantum Beam Science Directorate, Japan Atomic Energy Agency, 1-1-1 Koto, Sayo, Hyogo 679-5148, Japan*
[2]*Institute for Materials Research, Tohoku University, Sendai 980-8577, Japan*
[3]*Department of Physical Chemistry, University of Science and Technology Beijing, Beijing 100083, China*
[4]*Graduate School of Information Sciences, Hiroshima City University, Hiroshima 731-3194, Japan*
[5]*Department of Physics, Graduate School of Science and Technology, Kumamoto University, Kumamoto 860-8555, Japan*
[6]*Department of Chemistry and 4D LABS, Simon Fraser University, Burnaby, British Columbia, Canada V5A 1S6*

The local structures around Nb and Pb in the prototypical relaxor ferroelectric Pb(Mg$_{1/3}$Nb$_{2/3}$)O$_3$ (PMN) were investigated by x-ray fluorescence holography. The separate atomic images of nearest Pb around Nb revealed acute and obtuse rhombohedral structures of the crystal unit cells. The Pb-Pb correlated images showed a local structure of body-center-like $2a_0 \times 2a_0 \times 2a_0$ superlattice, proving a rigid three-dimensional network structural model combining the two kinds of rhombohedrons. The Pb atoms in the networks are positionally stable, while the other Pb atoms are fluctuating. This superstructure and the fluctuating Pb and Nb atoms are believed to play an important role in the relaxor behavior of PMN at the atomic level.

Nanoscale heterogeneous structures are known to play a crucial role in the appearance of gigantic susceptibilities and associated novel phenomena in solids; therefore, a direct method for determining nanoscale three-dimensional (3D) atomic arrangements of these systems is necessary. Relaxor ferroelectric behavior, which is characterized by a diffuse and frequency-dependent dielectric permittivity maximum in its temperature dependence, is a typical example. Relaxor ferroelectrics have attracted intense interest over the past few decades because of their complex local structure and puzzling mechanisms, as well as their potential use as high-performance electromechanical transducers based upon their excellent piezoelectric properties. A key commonly accepted structural concept in the relaxors seems to be the so-called polar nanoregions (PNRs) within a paraelectric (PE) matrix below the Burns temperature [1]. However, due to difficulties in dealing with the nanoscopic heterogeneity inherent in relaxors, the mechanisms of how PNRs appear and evolve upon cooling are not well understood, although several physical models have been proposed, such as the random-field model [2] and the dipole-glass model [3]. Therefore the role of PNRs in the outstanding piezoelectric properties of relaxor-based solid solution single crystals [4] has not been fully elucidated. In this work, we investigate a fundamental yet puzzling issue: the local 3D atomic arrangements around the Pb^{2+} and Nb^{5+} ions in the prototypical relaxor ferroelectrics Pb(Mg$_{1/3}$Nb$_{2/3}$)O$_3$ (PMN) [5,6] with the aid of a direct 3D and bulk sensitive technique, i.e., x-ray fluorescence holography (XFH).

PMN does not show any macroscopic phase transition down to 5 K, keeping an average cubic structure with the space group $Pm\bar{3}m$ and a lattice parameter $a_0 = 4.05$ Å [7]. Microscopically, however, nanoscale Mg-Nb chemically ordered regions (CORs; $Fm\bar{3}m$) [8–10] and their counterpart chemically disordered regions (CDORs; $Pm\bar{3}m$) exist as a PE matrix and PNRs ($R3m$ [11]) appear inside the matrix.

Neutron-scattering measurements can detect the diffuse scattering associated with PNRs, and also its basic components, i.e., the condensed soft transverse optical (TO) mode and the uniform phase shift [12–14]. Raman-scattering experiments have directly revealed that the TO-mode softening takes place not in CORs but in CDORs [9,15], whereas molecular dynamics simulations have provided little evidence that disorder affects the pattern of PNRs [16]. Furthermore, the concept of PNRs *in PE matrix* in relaxors has been questioned recently [17,18]. However, it is still unclear how the interplay between the TO mode and nanoscale disorder results in the formation of PNRs and phonon softening. Therefore, determining local-3D atomic arrangements is necessary to gain a better understanding of the local structures of relaxors.

XFH is a novel model-free technique for determining the 3D structure of local atomic arrangements around a specific fluorescing element [19,20] within a range of several nanometers at atomic resolution. XFH provides direct 3D structural information about the selected emitter element and its neighboring atoms. Moreover, XFH is sensitive to the fluctuation in composition, which is observable via the contrast of the atomic images. This method has been used to observe local lattice dynamics and atomic displacements in several functional materials, such as shape memory materials [21] and doped [22] and mixed crystals [23]. The 3D atomic arrangements are reconstructed in real space by Barton's multiple energy algorithm [24]. These features make XFH a method suitable for investigating nanoscale heterogeneous structures in solids.

In this Rapid Communication, two elements (*A*-site Pb and *B*-site Nb) were chosen for obtaining holograms to determine the local structure inside PMN. Single crystals of PMN were grown from high-temperature solution using PbO/B$_2$O$_3$ as flux [25]. A platelet of (001) orientation with dimensions of 3 × 4 × 1 mm^3 was prepared and polished to optical quality. The

---

*Present address: Toyota Technological Institute, Nagoya, 468-8511, Japan; gemini_huwen@hotmail.com

†khayashi@imr.tohoku.ac.jp

‡zye@sfu.ca
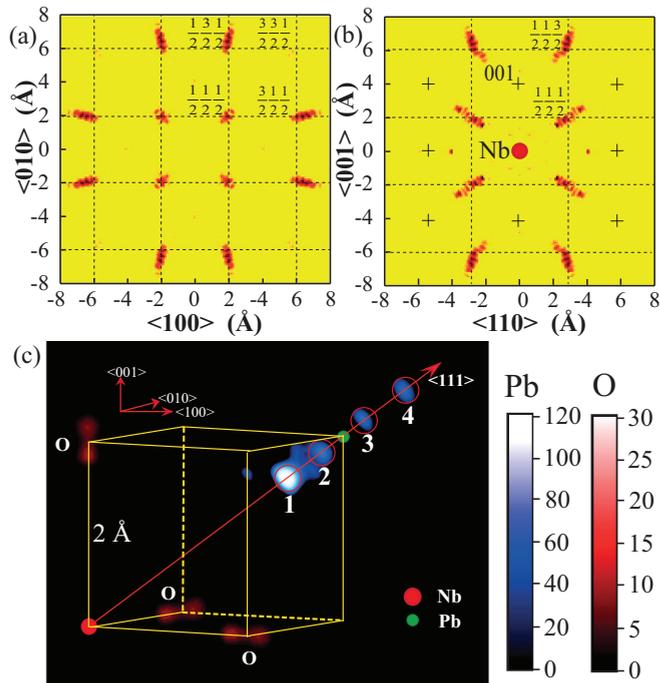
FIG. 1. (Color) Atomic images around Nb in $Pb(Mg_{1/3}Nb_{2/3})O_3$. (a) (001) plane at $z = 2$ Å and (b) (110) plane. Nb atoms are located 2 Å below the plane in (a) and at the center of (b). Intersections of dashed lines indicate the ideal positions of Pb atoms in (a) and (b). Crosses in (b) indicate the ideal positions of Nb/Mg. (c) 3D images of the nearest Pb and O atoms around Nb. The cube represents 1/8 of the unit cell. The blue and red color scales are the intensity scales of Pb and O atomic images. Green spot indicates the ideal position of Pb atom.

XFH experiments were carried out at beamline BL22XU of the SPring-8 synchrotron facility, Japan. The Nb $K\alpha$ and Pb $L\alpha$ fluorescent x-ray holograms were recorded using incident x-ray energies of 19.0–23.5 keV in 0.25 keV steps. Details are given elsewhere [26,27].

First, we discuss the real-space images from the Nb $K\alpha$ holograms. Figure 1(a) shows the atomic images of Pb on the (001) plane, 2 Å above the emitter Nb. The Pb atoms are clearly visible at the ideal positions. However, the intensity distributions in these atomic images are different from those in previously reported XFH images [27–29], which typically showed an isotropic distribution. The Pb images are elongated along the radial direction. The atomic images of Pb on the (110) plane are shown in Fig. 1(b). All of the Nb/Mg atoms on the *B* site are barely visible because these atoms are disordered; the image intensity of an atom is reduced by its fluctuations [30]. To confirm this, we calculated the theoretical holograms of $Pb(Mg_{1/3}Nb_{2/3})O_3$ using mean-square displacements of 0.3 and 0.1 Å for Pb and Nb/Mg, respectively [6]. The real-space images reconstructed from these holograms clearly show the Nb/Mg images. Therefore, we conclude that the degree of disorder of Nb/Mg is greater than previously reported value (0.1 Å). Pb atoms are visible around the emitter Nb because of the atomic correlation between the Pb and Nb atoms. Only the nearest Pb atoms exhibit ⟨111⟩ correlation with Nb.
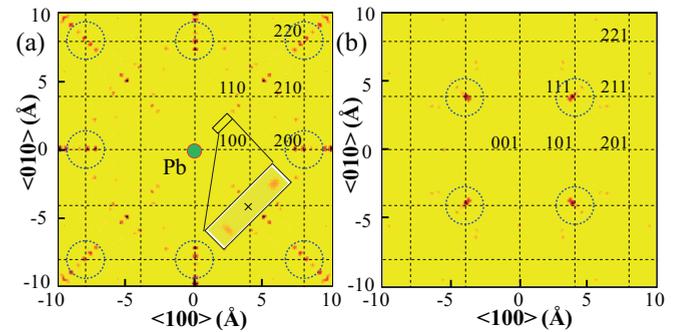
FIG. 2. (Color) Atomic images around emitter Pb on the (001) plane at (a) $z = 0$ Å and (b) $z = 4$ Å. Intersections of the dashed lines indicate the ideal positions of Pb atoms in (a) and (b). The center spot in (a) indicates the position of emitter Pb. Visible images are indicated by circles. The inset shows an enlarged view of the nearest O atomic images around Pb. The maximum contrast scale of the inset is half that of the other images.

Figure 1(c) shows a fine 3D image of first neighboring Pb and O atoms. Surprisingly, four Pb images are visible along the ⟨111⟩ direction, labeled 1–4 in Fig. 1(c). The interatomic distances between the central Nb and Pb1–4 are 2.73, 3.21, 3.71, and 4.25 Å, respectively. The Pb1 and Pb4 images show central symmetry about the ideal position (3.5 Å). As seen in Fig. 1(c), only the neighboring O images could be observed, and these are separated into two in the [100] direction with an interval of 0.25 Å. Splitting of the O position was also confirmed by x-ray absorption fine structure (XAFS) analysis [31].

Next, we consider the reconstructions from the Pb $L\alpha$ holograms used to evaluate the Pb-Pb correlation (Fig. 2). Because only the 200, 220, and 111 Pb atomic images are visible in Figs. 2(a) and 2(b), a body-center-like $2a_0 \times 2a_0 \times 2a_0$ superlattice structure emerged. The Pb atoms around the emitter Nb are more visible (Fig. 1), suggesting that the Pb atoms are positionally less stable than the Nb atoms. The atoms in Fig. 2(a) are separated along the radial direction. Thus, the Pb-Pb correlation might be discrete. Further analysis is in progress. The inset in Fig. 2(a) shows two Pb-O correlations at 2.3 and 3.4 Å, whereas no correlation was observed at the ideal position (2.85 Å), marked by the cross. The length scales are consistent with the pair distribution function (PDF) measurement [32] and with the static shifting of Pb cations with respect to O anions, which results in a *polarization*. The direction of the correlation along ⟨110⟩ may correspond to the anisotropy of the diffuse scattering at room temperature, namely, the *butterfly*-shaped diffuse scattering around $h00$ and the *ellipsoidal* diffuse scattering around $hh0$, where the distribution is mainly perpendicular to the ⟨110⟩ direction [18].

To ascertain what occurs at the atomic level, we focused on the following two anomalies: (1) the nearest Pb atomic images around Nb consist of four separate images and (2) the Pb atomic images around Pb show a body-center-like $2a_0 \times 2a_0 \times 2a_0$ superlattice.

The rhombohedral distortion explains well the separation of the Pb images in Fig. 1(c), and has been suggested for PMN by several techniques [7,11,33]. Our calculations show that the rhombohedral deformation of the perovskite cube with

rhombohedral angles of $77.0°$ and $100.6°$ gives rise to two Pb-Nb interatomic distance pairs of 3.23 and 4.22 Å, and 2.78 and 3.71 Å, respectively, which are close to the experimentally observed values. Therefore, we can conclude that there are acute and obtuse rhombohedrons in the local structure of PMN [Fig. 3(a)]. Here, we categorize the two inner/outer Pb atoms as long-displaced atoms (Pb1 and Pb4) and the other six Pb atoms as short-displaced atoms (Pb2 and Pb3) in order to simplify the discussion.

Because the cubic crystal symmetry is used, the short-displaced atoms along ⟨100⟩ appear at three different positions around the ⟨111⟩ axis. However, the experimental atomic images corresponding to these positions appear as an average only on the ⟨111⟩ axis. Thus, the rhombohedral shape is modified and the positions of the short-displaced atoms are closer to the ⟨111⟩ axis than to the ideal positions. Here, we can assume that the long-displaced atoms are positionally stable and that the short-displaced atoms fluctuate. To understand the Pb2 and Pb3 images in Fig. 1(c), we used a disklike two-dimensional (2D) Gaussian distribution with a mean-square displacement, σ_a.

The normalized intensities of Pb atoms 1–4 in Fig. 1(c) are 1, 0.75, 0.69, and 0.69, respectively. In order to reproduce these values, we calculated the image intensities of the short-displaced atoms by changing the value of σ_a. The calculated values with $\sigma_a = 0.19$ Å fit the experimental values well [26]. Moreover, we calculated the holograms using this parameter, and reconstructed the nearest Pb atomic images as shown in Fig. 3(b). The calculated atomic images are in good agreement with the experimental data, which indicates that there are two distorted rhombohedrons in PMN for the Pb-Nb correlations. The population ratio of acute and obtuse rhombohedrons was 1:1, whereas a_0 was kept constant in the calculation. The calculated σ_a value (0.19 Å) is smaller than that of displacement in a true rhombohedral structure (∼0.32 Å). We estimate that the atomic fluctuation of Nb atoms in PMN is around 0.19 Å.

Two Nb-Pb interatomic distances for short-displaced atoms (3.21 and 3.72 Å) were observed in the PDF analysis of the neutron powder diffraction data, whereas the long-displaced

FIG. 4. (Color) Structural model of the $2a_0 \times 2a_0 \times 2a_0$ superlattice constructed based on the combination of two kinds of local rhombohedral unit cells in PMN single crystal. Blue and red cubes correspond to acute and obtuse (distorted) rhombohedrons, respectively.

atoms were barely visible [11]. Because the intensity is proportional to the population of the atomic pairs in the PDF analysis, the correlations between Nb atoms and the six short-displaced Pb atoms were observed rather than those between Nb and the two long-displaced Pb atoms.

Then, we discuss the superlattice structure based on the results in Fig. 2. Combining the acute and obtuse rhombohedral unit cells, which are oriented alternately along the [111] directions, a body-center-like $2a_0 \times 2a_0 \times 2a_0$ structure can be constructed (Fig. 4). The positions of the Nb and Pb atoms shown in Fig. 3(a) are exchanged here so as to maintain the $2a_0 \times 2a_0 \times 2a_0$ Pb-Pb correlation. XFH provides 3D images relative to the emitter atoms; therefore, the data can be treated in this way. In forming this superlattice structure, the decrease in σ_a is important for the connections of the unit cells while maintaining the cubic symmetry on average. The connections at the short-displaced Nb/Mg atoms are shown as fuzzy shapes in Fig. 4. The XAFS study also confirmed the distortion of the Nb-Nb/Mg correlation and the large fluctuation of the Pb atoms [31]. Moreover, the lengths of the sides of the blue and red cubes are estimated to be 3.70 and 4.30 Å, respectively, which might affect the splitting of the Nb-O bond length.

However, this body-center superstructure conflicts with the face-centered symmetry ($Fm\bar{3}m$) for the CORs in the PE phase. The corresponding diffuse scattering around the M point [$= (\frac{h}{2}, \frac{h}{2}, 0)$] is very weak at room temperature [16]; the superstructure must exist on a very local scale. The estimated size of the domains is 1–2 nm, which is the same as the size of PNRs determined by diffuse scattering at room temperature [34]. The body-centered superstructure may be associated with the unusual phonon soft mode in PMN at the M point, as reported by Swainson *et al.* [35], indicating an underlying antidistortive transition from the cubic phase.

Our results show the network composed of acute and obtuse rhombohedrons, which indicates nanoscale antidistortive transformation. The polarization, namely, softened-TO mode

FIG. 3. (Color) Reproduction of the nearest Pb images around Nb, based on a rhombohedral transformation model of the unit cells. (a) Schematic of transformation of the unit cell from cubic to acute and obtuse rhombohedrons. σ_a is the FWHM of the 2D Gaussian distribution of Pb2 and Pb3 perpendicular to the [111] direction. (b) 3D images of the nearest Pb atom around Nb reconstructed from the calculated holograms with $\sigma_a = 0.19$ Å.

at the Γ point [9,15,36], should fluctuate under the influence of the potential from the antidistortive transformation. Therefore, our results suggest that competition between the antiferroelectric and ferroelectric correlations exists at room temperature, which is in agreement with the study published by Swainson *et al.* [35]. The local structure we observed is consistent with the idea of "soft" PNRs which contain a mixture of perovskite unit cells with permanently correlated dipole moments and unit cells with fluctuating moments arising from ferroelectric-antiferroelectric competition [37]. This competition is thought to be responsible for the interesting physical properties of relaxors, and our observations of the local structure of PMN support this directly.

In summary, the local structure of the complex perovskite relaxor ferroelectric PMN was investigated by XFH at room temperature. As demonstrated above, the atomic images reveal puzzling distorted rhombohedrons and a nanostructure composed of two sublattices. The first sublattice consists of positionally stable Pb and Nb ions and can be characterized by pseudorhombohedrons embedded in a body-center-like unit cell of size $2a_0 \times 2a_0 \times 2a_0$ with nonrhombohedral (possibly orthorhombic) symmetry. The second sublattice consists of off-centered Pb and Nb ions fluctuating around their corresponding ideal perovskite positions. No evidence was obtained for static polar nanoregions which should exist in PMN as continuous regions of ferroelectric order according to the conventional viewpoint. We suggest that fluctuating Pb and Nb ions are responsible for the characteristic broad relaxation spectrum observed in PMN.

This work expands the scope of XFH as a technique for characterizing disordered systems. As we have previously reported [21,23,30], XFH is sensitive to atomic fluctuation and distortion. Previous studies considered primarily the intensity of atomic images. We have demonstrated here that analyzing atomic image separation can provide more detailed structural information. This is a powerful tool for understanding the relationship between the properties and the local structures in disordered functional materials. So far, clear atomic images with fewer artifacts have been obtained up to a few nanometers. XFH is a unique method which is not only useful for probing medium-range (several nanometers) local structures, but also for many other structural characterizations yet to be developed. However, this method produces a large number of atomic images, particularly in disordered systems. The analysis of these images, which contain large amounts of information, can require substantial time and effort. The interpretation of the separate images beyond one crystal unit cell ($\sim$7 Å for a superlattice in PMN) is very difficult. Further development of XFH is necessary in order to interpret complex atomic images.

[1] G. Burns and F. H. Dacol, Solid State Commun. **48**, 853 (1983).

[2] V. Westphal, W. Kleemann, and M. D. Glinchuk, Phys. Rev. Lett. **68**, 847 (1992).

[3] E. V. Colla, E. Yu. Koroleva, N. M. Okuneva, and S. B. Vakhrushev, Phys. Rev. Lett. **74**, 1681 (1995).

[4] Z.-G. Ye, Mater. Res. Soc. Bull. **34**, 277 (2009).

[5] G. A. Smolenskii, V. A. Isupov, A. I. Agranovskaya, and S. N. Popov, Sov. Phys. Solid State **2**, 2584 (1961).

[6] A. A. Bokov and Z. G. Ye, J. Mater. Sci. **41**, 31 (2006).

[7] N. de Mathan, E. Husson, G. Calvarn, J. R. Gavarri, A. W. Hewat, and A. Morell, J. Phys.: Condens. Matter **3**, 8159 (1991).

[8] C. Boulesteix, F. Varnier, A. Llebaria, and E. Husson, J. Solid State Chem. **108**, 141 (1994).

[9] D. Fu, H. Taniguchi, M. Itoh, S. Y. Koshihara, N. Yamamoto, and S. Mori, Phys. Rev. Lett. **103**, 207601 (2009).

[10] I. Siny and C. Boulesteix, Ferroelectrics **96**, 119 (1989).

[11] I.-K. Jeong, T. W. Darling, J. K. Lee, Th. Proffen, R. H. Heffner, J. S. Park, K. S. Hong, W. Dmowski, and T. Egami, Phys. Rev. Lett. **94**, 147602 (2005).

[12] K. Hirota, S. Wakimoto, and D. E. Cox, J. Phys. Soc. Jpn. **75**, 111006 (2006).

[13] K. Hirota, Z.-G. Ye, S. Wakimoto, P. M. Gehring, and G. Shirane, Phys. Rev. B **65**, 104105 (2002).

[14] P. M. Gehring, S. Wakimoto, Z.-G. Ye, and G. Shirane, Phys. Rev. Lett. **87**, 277601 (2001).

[15] H. Taniguchi, M. Itoh, and D. S. Fu, J. Raman Spectrosc. **42**, 706 (2011).

[16] M. Paściak, T. R. Welberry, J. Kulda, M. Kempa, and J. Hlinka, Phys. Rev. B **85**, 224109 (2012).

[17] J. Hlinka, J. Adv. Dielectr. **2**, 1241006 (2012).

[18] A. Bosak, D. Chernyshov, S. Vakhrushev, and M. Krisch, Acta Crystallogr. A **68**, 117 (2012).

[19] M. Tegze and G. Faigel, Nature (London) **380**, 49 (1996).

[20] T. Gog, P. M. Len, G. Materlik, D. Bahr, C. S. Fadley, and C. Sanchez-Hanke, Phys. Rev. Lett. **76**, 3132 (1996).

[21] W. Hu, K. Hayashi, T. Yamamoto, N. Happo, S. Hosokawa, T. Terai, T. Fukuda, T. Kakeshita, H. Xie, T. Xiao, and M. Suzuki, Phys. Rev. B **80**, 060202(R) (2009).

[22] N. Happo, M. Fujiwara, K. Tanaka, S. Hosokawa, and K. Hayashi, J. Electron Spectrosc. Relat. Phenom. **181**, 154 (2010).

[23] S. Hosokawa, N. Happo, and K. Hayashi, Phys. Rev. B **80**, 134123 (2009).

[24] J. J. Barton, Phys. Rev. Lett. **67**, 3106 (1991).

[25] Z.-G. Ye, P. Tissot, and H. Schmid, Mater. Res. Bull. **25**, 739 (1990).

[26] See Supplemental Material at http://link.aps.org/supplemental/10.1103/PhysRevB.89.140103 for the details of the experimental procedure.

[27] K. Hayashi, N. Happo, S. Hosokawa, W. Hu, and T. Matsushita, J. Phys.: Condens. Matter **24**, 093201 (2012).

[28] M. Tegze, G. Faigel, G. Bortel, S. Marchesini, M. Belakhovsky, and A. Simionovici, J. Alloys Compd. **401**, 92 (2005).

[29] G. Faigel, G. Bortel, C. S. Fadley, A. S. Simionovici, and M. Tegze, X-Ray Spectrum. **36**, 3 (2007).

[30] S. Hosokawa, N. Happo, T. Ozaki, H. Ikemoto, T. Shishido, and K. Hayashi, Phys. Rev. B **87**, 094104 (2013).

[31] E. Prouzet, E. Husson, N. de Mathan, and A. Morell, J. Phys.: Condens. Matter **5**, 4889 (1993).

[32] W. Dmowski, S. B. Vakhrushev, I.-K. Jeong, M. P. Hehlen, F. Trouw, and T. Egami, Phys. Rev. Lett. **100**, 137602 (2008).

[33] R. Blinc, V. Laguta, and B. Zalar, Phys. Rev. Lett. **91**, 247601 (2003).

[34] G. Xu, G. Shirane, J. R. D. Copley, and P. M. Gehring, Phys. Rev. B **69**, 064112 (2004).

[35] I. P. Swainson, C. Stock, P. M. Gehring, Guangyong Xu, K. Hirota, Y. Qiu, H. Luo, X. Zhao, J.-F. Li, and D. Viehland, Phys. Rev. B **79**, 224301 (2009).

[36] S. Wakimoto, C. Stock, R. J. Birgeneau, Z.-G. Ye, W. Chen, W. J. L. Buyers, P. M. Gehring, and G. Shirane, Phys. Rev. B **65**, 172105 (2002).

[37] A. A. Bokov and Z.-G. Ye, Phys. Rev. B **66**, 064103 (2002).